JACS
JOURNAL OF THE AMERICAN CHEMICAL SOCIETY

Article

pubs.acs.org/JACS

Internal Photoemission in Molecular Junctions: Parameters for Interfacial Barrier Determinations

Jerry A. Fereiro,[†] Mykola Kondratenko,[†,‡] Adam Johan Bergren,*[,‡] and Richard L. McCreery*[,†,‡]

[†]Department of Chemistry, University of Alberta, 11227 Saskatchewan Drive Northwest, Edmonton, Alberta T6G 2G2, Canada

[‡]National Institute for Nanotechnology, National Research Council Canada, 11421 Saskatchewan Drive, Edmonton, Alberta T6G 2M9, Canada

Supporting Information

ABSTRACT: The photocurrent spectra for large-area molecular junctions are reported, where partially transparent copper top contacts permit illumination by UV−vis light. The effect of variation of the molecular structure and thickness are discussed. Internal photoemission (IPE), a process involving optical excitation of hot carriers in the contacts followed by transport across internal system barriers, is dominant when the molecular component does not absorb light. The IPE spectrum contains information regarding energy level alignment within a complete, working molecular junction, with the photocurrent sign indicating transport through either the occupied or unoccupied molecular orbitals. At photon energies where the molecular layer absorbs, a secondary phenomenon is operative in addition to IPE. In order to distinguish IPE from this secondary mechanism, we show the effect of the source intensity as well as the thickness of the molecular layer on the observed photocurrent. Our results clearly show that the IPE mechanism can be differentiated from the secondary mechanism by the effects of variation of experimental parameters. We conclude that IPE can provide valuable information regarding interfacial energetics in intact, working molecular junctions, including clear discrimination of charge transport mediated by electrons through unoccupied system orbitals from that mediated by hole transport through occupied system orbitals.

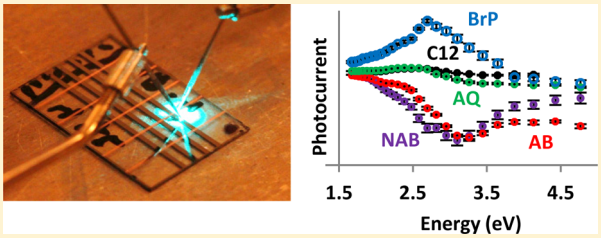

INTRODUCTION

Molecular electronics can be broadly defined as the study of charge transport across molecular distances (generally less than ∼10 nm), including potential applications in microelectronics. Part of the motivation for the genesis of this field is the conceptual extension of Moore's law, where it was realized that extending the ever-decreasing size of integrated circuits would eventually result in individual devices with molecular size.[1,2] However, while the decreasing miniaturization of electronic components is often described as the primary motivator in molecular electronics, there are other important reasons for investigating molecules as circuit components. Another strong motivation includes using the vast array of organic structures to achieve functions that are difficult with conventional semiconductors. While electronic devices consisting of single molecules bridging two conducting contacts have been fabricated and studied,[3−9] molecular junctions that occupy relatively large areas (e.g., ∼200 × 200 μm^2) have also become an important platform for studying molecular electronics.[3,10−12] In order to enable the application of molecular devices in any real-world setting, a fundamental understanding of the factors that control their conductance and its dependence on molecular structure is required.

Given the prospect of using organic molecules as working functional components in electronic devices[13] and the enormous value of the current global electronics industry, the field of molecular electronics has become an active area of international research. Significant advances in understanding transport have been made over the past decade,[2,3,14−20] and various platforms have been developed to study the electrical characteristics and charge transport mechanism(s) in molecular junctions.[6,21,22] Despite these advances, a clear understanding of all of the factors that govern conductance in a molecular junction has been elusive, in part because the electronic properties of molecules may vary over a wide range, from insulating to conducting. Moreover, it has become clear that interactions between the molecules and conductors in a molecular device lead to the requirement to consider a molecular junction as a system, where the properties of the individual, isolated components are insufficient or misleading for predicting the behavior of a completed device.[23,24] Since the specific design of electronic function has been a primary goal in molecular electronics,[12,25] information regarding system energy levels in complete, functioning devices, including possible interactions between the molecules and the contacts, is critical to further progress. Several recent reports on in situ characterization of molecular junctions have been published, including UV−vis,[26,27] infrared[28−31] and Raman spectroscopy,[32,33] thermopower measurements,[34,35] and inelastic tunnel-

Received: November 11, 2014

DOI: 10.1021/ja511592s
J. Am. Chem. Soc. XXXX, XXX, XXX−XXX

ing spectroscopy.[33,36,37] While these methods provide information about junction structure and carrier sign, they do not directly probe system energy levels. Other measurements that do provide knowledge regarding energy levels (e.g., ultraviolet photoelectron spectroscopy[38,39]) are not readily carried out on completed devices.

Illumination by photons in the ultraviolet and visible range of the spectrum can result in transitions between electronic states that involve HOMO−LUMO transitions in molecules, as well as the excitation of carriers across moderate to large interfacial barriers. Such barriers in many molecular electronic systems reside in the 1−3 eV range,[24] corresponding to wavelengths ∼400−1240 nm. From this general discussion, it is clear that, in the specific case of a large area molecular junction composed of an organic molecule between two conductors, illumination can induce conduction through excitation of carriers in the contacts or of electrons within orbitals in the molecular component. Characterization of these photocurrents therefore can reveal information regarding the energy levels within molecular junctions. However, since there are different pathways for generating photocurrent, the relationship between energy levels within molecular junctions and the resulting photocurrent is not obvious.

One form of photocurrent spectroscopy that has been employed in the past for characterization of internal energy levels in metal−insulator−metal (M−I−M) junctions is internal photoemission (IPE), which is a variation on the classical photoelectric effect. In external photoemission, a photon-induced electronic excitation in a solid conductor leads to carriers with energy greater than the work function of the conductor, and electrons are injected into a vacuum. However, in IPE in a solid-state junction, the photon energy is lower than the contact work function, but can be high enough to inject carriers into or across an internal energy level, resulting in a measurable current across the junction. IPE has been used to measure barrier heights in various M−I−M junctions (where "I" is typically an oxide tunneling barrier), notably across aluminum oxide tunnel junctions.[40−43] We previously showed preliminary data[44] that indicated IPE could be used to characterize the interfacial barrier of molecular junctions consisting of carbon/molecule/Cu, with the energy threshold for photocurrent indicating the $E_f - E_{HOMO}$ or $E_{LUMO} - E_f$ interfacial barriers (where E_f is the system Fermi level). We also reported that the sign of the photocurrent can provide information regarding the involvement of the HOMO or LUMO in mediating tunneling across the molecular junction.

In this paper, we extend our previous results to a wider range of molecular structures, and explore the use of IPE to characterize energetics in molecular junctions. Through systematic correlation of the photocurrent spectrum with that of the absorbance spectrum of different molecules, plus variation of the molecular layer thickness, source intensity, and photon energy, we identified photocurrents resulting from photon absorption in the contacts and those induced by photon absorption in the molecular layer. The results permit formulation of criteria for determining the origin of the photocurrent, and the relationship to the position of system energy levels. For molecular junctions that show only IPE-based photocurrent, an analysis through construction of a Fowler plot can yield a measurement of the interfacial barrier, where the photocurrent sign can be used to determine whether electron or hole transport is dominant. IPE was characterized and illustrated with molecular junctions made with seven different aromatic, aliphatic, and organometallic molecular junction structures, which exhibit conduction mediated by both occupied and unoccupied system orbitals.

EXPERIMENTAL SECTION

The schematic of the junction structure and the structures of all the molecules used in this study are provided in Supporting Information (SI), Figures S1 and S2. Molecular layers included azobenzene (AB), anthraquinone (AQ), bromophenyl (BrP), nitroazobenzene (NAB), phenyl ferrocene (Fc), dodecylamine (C12), and naphthalene diimide (NDI), all of which were multilayers on pyrolyzed photoresist film (PPF) substrates with the their thicknesses determined with AFM (in nm): for example, AB(3.4 nm), BrP(3.0 nm). The fabrication of molecular junctions has been described in detail previously,[22,24,44−47] and utilizes the electrochemical reduction of diazonium reagents on flat carbon surfaces[48] and vapor deposition of metallic[22] or carbon[49] top contacts. However, rather than silicon substrates with an insulating layer of thermal oxide, polished fused quartz substrates (from Technical Glass Products, Inc.) were used as a substrate in the current study to avoid the possibility of stray photocurrent from crystalline silicon. For the $Al/Al_2O_3/Cu$ junctions, polished borosilicate glass was first cleaned by sonication in acetone followed by IPA and water for 10 min each, then 60 nm of Al was deposited via e-beam evaporation through a shadow mask with a 3 nm Cr adhesion layer. Next, the samples were heated in air to a temperature of 175 °C (verified using an IR thermometer) for 10 min. Finally, 20 nm Cu was deposited using a shadow mask oriented perpendicular to the Al/Al_2O_3 lines.

As illustrated in the schematic representation of the optical apparatus[44] in Supporting Information Figure S1, photocurrent spectra were measured by passing a small band ($\Delta\lambda$ = 13 nm) of light from a Xe arc source and monochromator through an optical chopper and onto the junction. Lock-in detection (Supporting Information Figure S3-A) was used to measure the resulting photocurrent, and an independent measure of the optical power incident on the junction with a Newport 1936-R power meter was used to determine the external quantum yield (EQE).[44] EQE is defined as the number of photoelectrons in the external circuit divided by the number of photons incident on the junction. The sign of the photocurrent was determined by calibrating the phase of the lock-in detection using a photodiode as a reference, as described previously,[44] where a positive photocurrent indicates electrons flowing from the Cu to PPF in the external circuit. Laser diodes operating at 808 nm (1.53 eV) and 852 nm (1.46 eV) from Thorlabs were used to extend the photocurrent measurements beyond the useful range of the Xe arc.

The photocurrent sign was also verified with laser illumination and dc current measurements in several cases (Supporting Information Figure S3-B) to avoid any ambiguity resulting from phase sensitive detection. In order to measure photocurrent as a function of incident power, laser light from an Ar-ion laser was directed onto the junction, which permitted the use of direct current measurements and a wider range of incident power than that available with the Xe arc source. The optical power delivered to the junction was determined immediately above the sample with the Newport power meter, and the focused spot size was determined visually. The power density at the junction varied from 0.6 to 7 W/cm^2 for Xe arc illumination and up to 50 W/cm^2 for laser illumination, and the resulting photocurrents were stable for many hours. In all cases, at least four junctions on a given chip were studied in order to determine the standard deviation of the photocurrent.

RESULTS AND DISCUSSION

Figure 1 shows a schematic energy level diagram for a molecular junction. This model is based on the availability of electronic states, represented by horizontal lines, where shading represents occupied states in the conducting contacts. The Fermi level (E_f) of the contacts (defined as the energy where the probability of finding an electron is 0.5) therefore

DOI: 10.1021/ja511592s
J. Am. Chem. Soc. XXXX, XXX, XXX−XXX

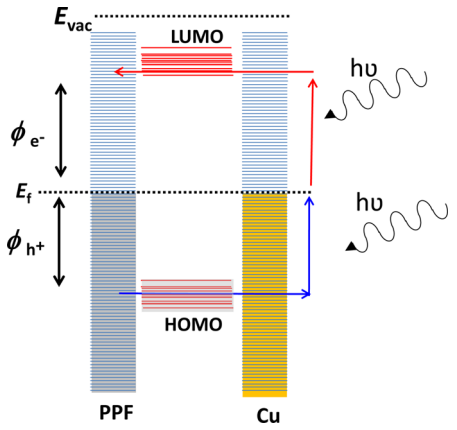

Figure 1. Energy level diagram showing a nonresonant tunnel barrier for holes (HOMO-mediated transport, blue arrows) and electrons (LUMO-mediated transport, red arrows).

represents the demarcation between filled and empty states for the conductors, while the molecular component has filled (HOMO) and empty (LUMO) orbitals. The gap between the frontier orbitals in the molecular region (i.e., the HOMO−LUMO gap, E_g) creates a region where electrons are not allowed so that when these orbitals are separated from E_f by an energy greater than kT, carriers cannot pass freely from one contact into the other, resulting in an interfacial barrier for electrons (ϕ_{e^-}; LUMO-mediated transport) and holes (ϕ_{h^+}; HOMO-mediated transport). In cases where the distance between the two conductors is small, ϕ is a nonresonant quantum mechanical tunneling barrier. Multiple values of molecular orbitals are shown to represent inhomogeneous broadening by the various orientations in the molecular multilayer.

While the model in Figure 1 has been used in numerous descriptions of molecular junctions, there are several issues that are not readily apparent in this diagram. For example, strong electronic coupling between the contacts and molecular layer can result in a dipole across the interface that can be important in determining the actual system barrier (i.e., an electrostatic dipole barrier results from partial charge transfer between the molecule and contact).[24,50,51] Moreover, interactions between the molecule and contacts can lead to hybridization, creating orbitals that span both the molecule and the contact(s). These effects can result in a distribution of highest occupied (HOSO) and lowest unoccupied (LUSO) *system* orbitals with significantly different energies from the free-molecule HOMO or LUMO levels, as well as shifts in the local vacuum level over the molecular layer.[51,52] As will be discussed below, the orbital energy levels relevant to transport in the junction are not those for isolated molecules but instead are the occupied system orbitals (HOSOs) and unoccupied system orbitals (LUSOs) which incorporate electronic changes during fabrication. For all of these reasons, methods that provide energy level alignment and barrier height information in intact, complete junctions are highly valuable.

We previously reported that IPE can provide a direct measure of both the hole ($E_f - E_{HOSO}$) and electron ($E_{LUSO} - E_f$) tunnelling barriers, although this analysis is complicated by IPE currents from both the contacts and additional photocurrent from excitons resulting from optical excitation of the molecular component.[44] The generation of photocurrent by an IPE mechanism is initiated by light absorption in the conducting contacts[40,43,53−55] and results in hot electrons through the excitation and decay of surface plasmons.[56−58] These nonequilibrium carriers can then traverse the molecular layer and be collected at the second electrode when the photon energy exceeds the interfacial barrier (i.e., such that the carrier energy is resonant with the orbital energy) and if energy losses due to scattering are minimal. To illustrate how IPE might provide both hole and electron barriers, Figure 1 shows light-stimulated hole transport (blue arrows), where an electron from an occupied state in one contact (here shown as carbon) is transferred to a photogenerated hole in the other contact (here, Cu), resulting in a positive shift in the PPF potential and a positive photocurrent in the external circuit. The red arrows indicate the excitation of an electron, which is transported via a LUSO to the carbon, producing a negative photocurrent. Thus, hot carriers can cross both hole and electron tunnelling barriers,[53] resulting in either positive or negative photocurrents, thus serving as an indication of both occupied and unoccupied states in the barrier region.

While IPE relies on excitation of carriers in the contacts, the overall photocurrent for a given molecular junction may have contributions from other mechanisms where the photon is absorbed by the molecule rather than the contacts. For example, the illumination of organic molecules within a molecular junction can generate excitons which dissociate and result in a photovoltaic response in addition to IPE. In this report, we have two primary goals: first, to determine ways to distinguish IPE from other photocurrent-generating mechanisms; and second, to use IPE to characterize energy level alignment and barrier heights in molecular junctions. In order to provide a test-bed for investigating IPE, we have identified several molecules that have different absorption spectra, and have tested the dependence of the photocurrent on several parameters, including molecular structure, molecular layer thickness, source intensity, and energy, as discussed below.

Theoretical descriptions of the IPE process are based on Fowler theory,[59] such that the IPE photoemission yield (Y, photoelectrons/incident photon) is given by[53,60]

$$Y \propto (E - \phi)^2 \quad (1)$$

where E is the incident photon energy ($h\nu$ where h is Planck's constant and ν is frequency), and ϕ is the interfacial barrier, e.g., $E_{LUSO} - E_f$. A plot of $Y^{1/2}$ versus photon energy (i.e., a Fowler plot) is expected to be linear if IPE is the only process involved in photocurrent generation, and linear extrapolation of the Fowler plot to the x-axis can be used to determine the value of the interfacial barrier height. Equation 1 and Fowler theory should not be confused with field emission (also known as Fowler−Nordheim tunneling). Although Fowler developed theories for both phenomena, they are completely distinct, and we are concerned here only with understanding the photocurrent response. Augmentation of IPE by optical absorption in the molecular layer has been described as "pseudo-IPE" in the case of thick molecular layers on conductors.[53] This additional photoeffect is distinct from IPE and will be discussed only briefly here, although the ability to use IPE to characterize molecular junctions requires identification and avoidance of pseudo-IPE.

In order to provide ways to identify IPE, several experiments were carried out, including measurement and analysis of the photocurrent in molecular junctions with a broader range of molecular structures and layer thicknesses than in our initial report.[44] The optical absorbance of each molecule bonded to

DOI: 10.1021/ja511592s
J. Am. Chem. Soc. XXXX, XXX, XXX−XXX

the PPF substrate was determined and compared to the observed photocurrent spectra to determine the effects of molecular absorption. These criteria enable a full assessment of what information IPE can provide regarding energy levels in functioning molecular electronic devices.

In order to provide a baseline that is free from molecular absorbance, we will start by discussing the photocurrent spectrum of Al/AlOx/Cu junctions and a carbon/C12/Cu junction (C12 and AlOx do not absorb light in this 200−800 nm spectral range). The measured photocurrent yield (i.e., the number of electrons per incident photon after calibration of the light intensity) as a function of photon energy for both junctions is shown in Figure 2A.

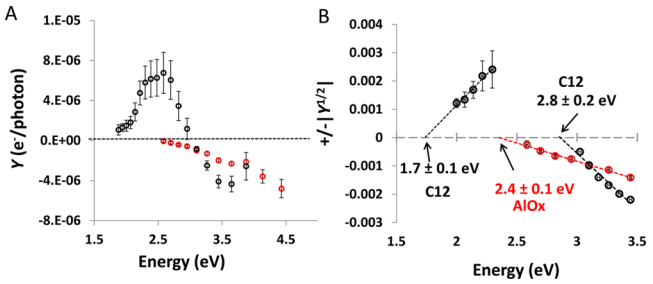

Figure 2. (A) Photocurrent yield spectra for two junctions (Al/AlOx/Cu, red curve, and carbon/C12/Cu, black curve). (B) Corresponding Fowler plots with extrapolated barrier values. C12 data is from a previous report.[44]

The negative photocurrent measured for the AlOx junction indicates that the Al substrate becomes negative when illuminated, such that photoexcited electrons in the copper traverse the oxide through its conduction band. The opposite sign for the case of the alkane junctions (black curve) at low energy results from electron transport through the HOSO into photogenerated holes in the Cu contact, as reported previously[24,44] and shown schematically in Figure 1.

Figure 2B shows a Fowler plot for an Al/AlOx/Cu(20 nm) junction, where the extrapolated value of the electron tunneling barrier is determined to be 2.4(±0.1) eV, consistent with other reported values. Although a range 0.9−3 eV, e.g., has been reported, Goodman reported a value of 2.0 ± 0.2 eV for electrons in AlOx exposed to liquid water.[43] As reported previously, and is apparent in Figure 2B, the hole tunneling barrier ($E_f - E_{HOSO}$) for a PPF/alkane/Cu junction is 1.7(±0.1) eV and $E_f - E_{LUSO}$ is 2.8(±0.2) eV, respectively, both based on the Fowler plot intercept. In the cases shown in Figure 2A, absorbance by the molecular portion of the junction is avoided by the choice of materials. However, molecular electronics involves the use of a wide range of structures with varied optical absorption characteristics. Below, we describe how the absorption spectrum of a molecule correlates with the photocurrent spectrum for a series of molecules.

The structures of five different organic molecules (AB, NAB, AQ, BrP, and C12) are shown in Supporting Information Figure S2, and have all been used previously to construct molecular junctions of the structure carbon/molecule/Cu (20 nm).[24] Figure 3A shows a plot of the photocurrent yield as a function of photon energy for five different molecular structures with approximately equal molecular layer thicknesses, as follows: C12 (2.3 nm, black curve),[44] BrP (3.0 nm, blue curve),[44] AQ (2.5 nm, green curve), AB (3.4 nm, red curve), and NAB (4.0 nm, violet curve). Notable observations from

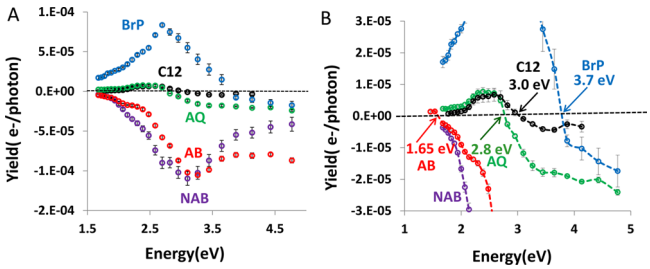

Figure 3. (A) Photocurrent yield spectrum for five different junctions [BrP (blue curve), C12 (black), AQ (green), AB (red), and NAB (violet)]. (B) The same data on an expanded *Y* axis, with the photon energies indicated where the curves cross the *X* axis.

Figure 3A include a similar photoresponse for C12 and AQ at low energy (<2.8 eV), while a larger and negative photocurrent is observed for the AQ junction above 3 eV. The magnitude of the yield for junctions containing AB and NAB molecules at low energy (<2 eV) is comparable to that of C12 and AQ, but at higher energies, the yield for these two molecules increases significantly, and is negative. We previously proposed[44] that the change in sign for the C12 junction was indicative of the smaller interfacial barrier defined by the HOSO being more energetically accessible than the LUSO. Thus, the photocurrent at low energies is positive, but becomes negative when the electron tunneling barrier becomes accessible. This enabled the energy level alignment of electron and hole barriers for the C12 junction to be determined.[44]

Note that in Figure 3A the energy where the photocurrent changes sign (i.e., the "crossing point" of the plot in Figure 3B) depends on the structure of the molecule: the crossing points are 3.7 eV for BrP, 2.8 eV for AQ, 1.65 eV for AB, while NAB remains negative in the spectral range studied and does not cross the abscissa. In order to determine if the absorbance of the molecule correlates with these crossing points, the photocurrent yield spectra are overlaid with the absorbance spectra for each of the aromatic molecules in Figure 4 (complete details for obtaining absorbance spectra for the thin molecular layers on carbon are provided in Supporting

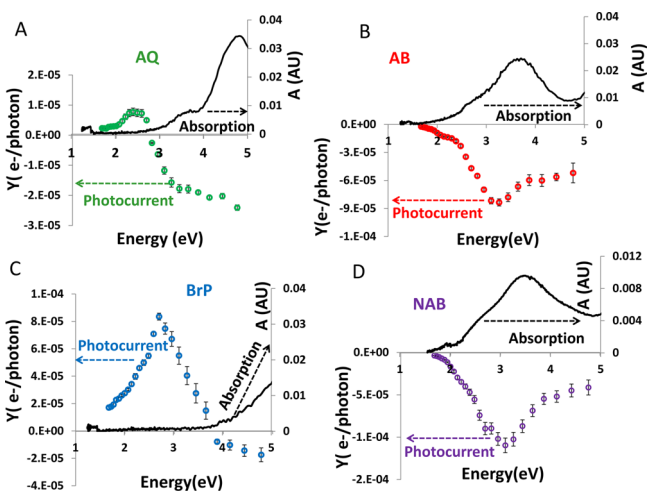

Figure 4. Overlay of photocurrent yield and absorption spectra for four different junctions; black line indicates the optical absorption spectra of the molecular layer corrected for PPF absorption, and the colored line indicates the measured photocurrent spectrum of a particular molecule (A) AQ, (B) AB, (C) BrP, and (D) NAB.

DOI: 10.1021/ja511592s
J. Am. Chem. Soc. XXXX, XXX, XXX−XXX

Table 1. Summary of Optical Absorption Data for Molecular Layers

energy (eV)	BrP	AQ	AB	NAB	C12
free molecule, DFT (HOMO−LUMO)	6.2	4.2	3.9	3.6	7.8
UV−vis peak, solution	>6	∼4	3.9/2.7s[a]	3.7/2.7s	>6
UV−vis absorption onset	5.2	3.6	3.4/2.4s	3.2/2.3s	
PPF-bonded peak	>6	4.8/3.6s	3.6/2.5s	3.4/2.5s	>6
PPF-bonded onset	3.6	2.5	1.7	1.7	>6
PC crossing point	3.7	2.8	1.6	<1.46	3.0

[a]s indicates shoulder on main UV−vis absorption peak.

Information, section 4[61]). Here, a striking relationship between optical absorbance (black curves) and the measured photocurrent yield spectra (colored data points) implies that absorption by the molecular component plays a role in determining the photocurrent spectrum characteristics, notably the abscissa crossing energy and the onset of negative photocurrent. In Figure 4A, it is apparent that the magnitude of the photocurrent for AQ is similar to that of the alkane junction (see Figure 3B) in the energy range where little or no absorption by AQ takes place (below ∼2.5 eV). However, at higher energies, when the AQ crosses the abscissa and becomes progressively more negative, the AQ photocurrent significantly exceeds that of the alkane. One possible explanation is that when the molecule does not absorb incident light, IPE is the main mechanism contributing to the photocurrent, and the positive photocurrent indicates that the HOSO mediates the tunneling process for both molecules (i.e., it is more energetically accessible). When the molecule absorbs light, a secondary mechanism contributes additional negative current to the photoresponse. Recalling from Figure 3B that the AQ molecule photocurrent crossing point is 2.8 eV, we note that the onset for optical absorption for AQ chemisorbed to a transparent carbon surface is 2.5 eV (see Supporting Information Figure S5-B). A similar analysis of absorption and abscissa crossing energy was done for each molecule in Figure 3B, as well as C12, and is summarized in Table 1. It is important to note that while optical absorption onset and electron transport barriers provide important information about junction electronic structure, they are derived from different processes, and cannot be directly connected without taking into consideration several different factors.[62]

In the case of AB and NAB, where significant optical absorption occurs even at low energy, the photocurrent measured using the continuum light source remains negative throughout the entire accessible spectral range of the Xe arc (see Figure 4B,D). Either there is no photocurrent crossing point for these molecules, or it cannot be observed using the continuum source, due to its limited power. However, using laser diodes allows sufficient power to enable the measurement of the photocurrent at lower photon energies. The two points (808 and 852 nm) obtained from these measurements both resulted in positive photocurrent for the AB junction, and are included in the AB photocurrent spectrum in Figure 3B, showing that the crossing point for AB is ∼1.6 eV. Analysis of the compiled data in Table 1 clearly shows that the photocurrent crossing point correlates with the onset of optical absorbance for the four molecules where both are available. This result indicates that a two-regime model is needed to explain the entire photocurrent spectrum for certain molecules: an IPE regime at low energies where molecular absorption is negligible, and a second photocurrent mechanism involving molecular absorption (MA) at higher energies, with the particular crossing point dictated by molecular structure. The conclusion from analysis of Table 1 is that in order to use IPE to characterize energy levels while avoiding interference by a molecular absorption photocurrent the analysis must be done in a region where the observed photocurrent is dominated by IPE. In order to provide additional tests of the contribution of molecular absorption, we examined the dependence of the photocurrent on excitation intensity and the molecular layer thickness.

As noted above, IPE current is characterized by excitation of surface plasmons in the contacts, which decay into hot electron−hole pairs, with subsequent transport across internal system barriers at appropriate energies. Because conductors have very high carrier concentrations, the excitation of hot carriers is linearly dependent upon the excitation source intensity as long as the number of the excited carriers is small compared to the total number of carriers present. Thus, the IPE photocurrent is expected to increase linearly with excitation intensity over a wide range of intensity. However, exciton formation in molecular materials can show nonlinearity for at least two reasons. First, the density of molecular ground states may be depleted faster than they can refill at high excitation levels. Second, various models of exciton generation include a nonlinear term due to recombination effects. In particular, bimolecular and/or surface recombination is expected to result in proportionality between the square of the photocurrent and the excitation intensity.[59,63,64] Following a previously reported derivation for exciton generation,[63] the number of excitons (n) and the resulting photocurrent are linearly dependent on the illumination intensity (I, in photons/sec), given by eq 2

$$n = \alpha I \tag{2}$$

where α is a constant representing optical absorption in the material. Next, we define the rate constant for monomolecular recombination (k_m) as being inversely related to the lifetime of the mobile charge carrier optically generated in the material. In the case of IPE, an optically generated hot electron in Cu crosses the barrier and undergoes recombination with a nonmobile hole in the carbon contact. Here, the process of a single mobile charge carrier annihilating a localized positive charge in the carbon contact makes the carbon more negative, and represents a monomolecular process since a single mobile charge carrier is eliminated. For the case of two mobile charges (bound or not) recombining, we define a rate constant k_b, the bimolecular recombination rate constant. Since the steady-state condition gives the rate of change of n with respect to time as zero, we have

$$\alpha I - mn - bn^2 = 0 \tag{3}$$

when n is small relative to the total number of available states

DOI: 10.1021/ja511592s
J. Am. Chem. Soc. XXXX, XXX, XXX−XXX

$$n = \frac{\alpha}{m} I \tag{4}$$

and when n is large relative to the available states

$$n = \sqrt{\frac{\alpha I}{b}} \tag{5}$$

Equation 4 shows that when the photocurrent is controlled by monomolecular recombination, such as a hot carrier crossing a barrier and being collected by a second electrode,[63] the photocurrent will be a linear function of intensity. This is true as long as the number of excited carriers is small relative to the number of carriers in the contact (i.e., carriers in the conductor are not able to be exhausted by the excitation process). This assumption is reasonable since Cu has a high carrier density, and the measured photocurrent is small. Thus, IPE is expected to remain linear with excitation intensity over a wide range of experimental conditions. Equation 5, on the other hand, shows that bimolecular recombination is expected to exhibit a photocurrent that is proportional to the square root of intensity. In this instance, the total number of excited carriers now can be relatively large relative to the number of available states in the molecular layer. These considerations imply that a good test of mechanism is the relationship between photocurrent and excitation intensity.

Given the mechanistic inferences from Figure 4, the response to a particular incident wavelength can be predicted to be linear or quadratic. For example, at photon energies below 3.0 eV, AlOx, BrP, and AQ junctions are expected to show linear photocurrent vsintensity plots, since the molecules do not absorb light and the dominant mechanism is IPE. In contrast, AB absorbs light over the range 1.7−3 eV, and is expected to show a nonlinear dependence on intensity. Figure 5 shows plots of the photocurrent (i_p) as a function of the excitation intensity for several different junctions under constant (i.e., unmodulated) laser illumination at selected optical energies. First, Figure 5A shows a plot for the Al/Al_2O_3/Cu (20) sample, for which a negative dc photocurrent was recorded using a picoammeter (see Supporting Information for more details)

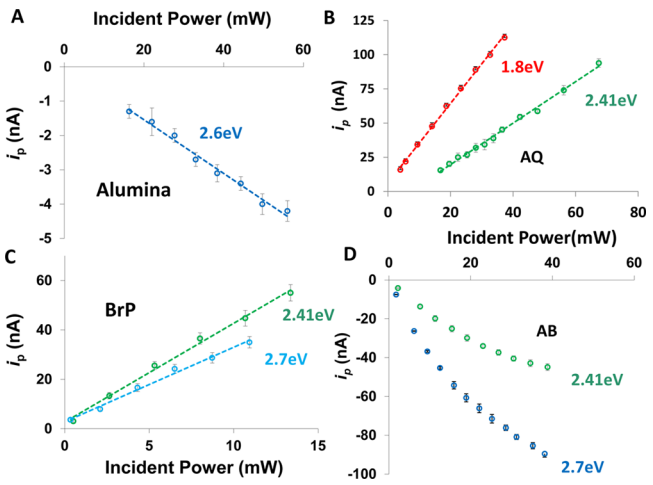

Figure 5. Photocurrent vs light intensity curves for (A) Al/AlOx/Cu, blue curve at 2.6 eV (476 nm); (B) carbon/AQ/Cu at 1.8 eV (688 nm), red curve, and 2.4 eV (516 nm), green curve; (C) carbon/BrP/Cu at 2.4 eV (516 nm), green curve, and 2.7 eV (458 nm), blue curve; (D) carbon/AB/Cu at 2.4 eV (516 nm), green curve, and 2.7 eV (458 nm), blue curve.

and Ar-ion laser illumination at 475 nm (2.65 eV). The photocurrent response is linear with excitation intensity, as expected for a pure-IPE derived photocurrent. Since AlOx does not have any optical transitions within the energy region tested, it provides an excellent control experiment and confirms the linearity of IPE current with intensity. Second, Figure 5B shows a similar plot for an AQ-containing junction which exhibits linear response for both 514 nm (2.41 eV) and 689 nm (1.80 eV), as predicted from Figure 4A given the weak absorbance of AQ at these wavelengths. Third, Figure 5C shows the analogous plots for BrP at 2.4 and 2.7 eV, again displaying a linear increase with intensity as expected from Figure 4C. It is also important to note that the sign of the photocurrents from Figures 4 and 5 match, such that, in cases where no absorption takes place, the photocurrent is negative, indicating LUSO mediated transport (Al_2O_3) or positive indicating HOSO transport (AQ and BrP) where expected. Taken together, the results for AlOx, AQ, and BrP in Figure 5A−C indicate that the observed photocurrent is dominated by IPE, with negligible contribution from photon absorption in the molecular layer. Finally, the AB molecular layer does show significant absorbance below 3 eV, and plots of i_p versus excitation intensity for two wavelengths (458 nm, or 2.7 eV; and 514 nm or 2.4 eV) where AB absorbs light are shown in Figure 5D. Here, the photocurrent is negative and displays a clear nonlinear trend. This sublinear increase of the photocurrent with intensity is consistent with a simple quadratic function, showing that when the molecule absorbs a significant amount of the incident light, the photocurrent is governed by a bimolecular recombination mechanism (eq 5) that is distinct from IPE. To confirm this hypothesis, we also monitored photocurrent versus intensity for alkane junctions at 2.4 and 2.7 eV (Figure S6 in Supporting Information), and in both cases the plots were linear. Overall, the dependence of the photocurrent on excitation intensity enables determination if IPE is the dominant mechanism or if molecular absorption contributes significantly.

In order to obtain further insight into the IPE regime of the photocurrent spectra, we examined molecular junctions containing ferrocene and NDI molecular layers. These molecules exhibit very weak optical absorption below 3 eV (Figure 6A,B, solid lines and right ordinate), which leads to the expectation that IPE should dominate the photocurrent spectra for these molecules below 3 eV. Figure 6A,B shows overlays of the absorption and photocurrent spectra as functions of photon energy for molecular junctions containing ferrocene and NDI, respectively. Figure 6A shows that the photocurrent measured for a Fc junction is positive throughout the entire spectral range, indicating that the HOSOs mediate transport for the IPE mechanism. However, at energies above 3 eV, the photocurrent yield decreases in magnitude. One possible explanation for this observation is that above 3 eV the secondary mechanism (i.e., MA) might significantly exceed the primary IPE mechanism. A second possibility is that LUSO-mediated IPE begins contributing to the overall current, acting to decrease the overall yield. Figure 6B shows a photocurrent spectrum for an NDI molecular junction that is similar to that observed for Fc junctions, except that the photocurrent for NDI is always negative. The lack of molecular absorbance in this region implies that both Fc and NDI photocurrents are due to IPE, and that they are HOSO and LUSO mediated, respectively. Figure 6C,Ds show the photocurrent dependence on incident light intensity for two energies for both Fc and NDI. In all four

DOI: 10.1021/ja511592s
J. Am. Chem. Soc. XXXX, XXX, XXX−XXX

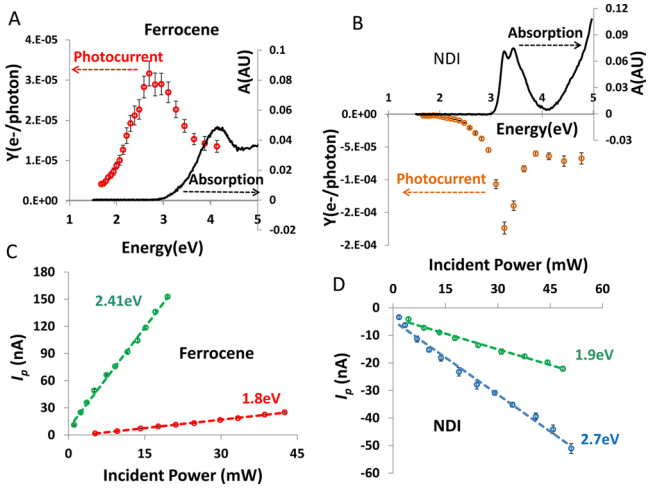

Figure 6. Overlay of photocurrent yield (colored lines) and absorbance spectra (black lines), for (A) Fc and (B) NDI. (C) Photocurrent vs intensity for PPF/Fc/Cu at 2.4 eV (green line), and 1.8 eV (red). (D) Photocurrent vs intensity for PPF/NDI/Cu at 2.7 eV (blue) and 1.9 eV (green).

cases, the photocurrent is linear with intensity, as expected for IPE without significant molecular absorption.

An additional mechanistic test for a MA contribution is the variation of the photocurrent with the thickness of the molecular layer. The IPE mechanism should show a weak dependence on the thickness of the molecular layer, at least up to the scattering length of electrons in the molecular layer. Any mechanism involving optical absorption by the molecular layer should increase linearly with layer thickness. Figure 7A,B shows

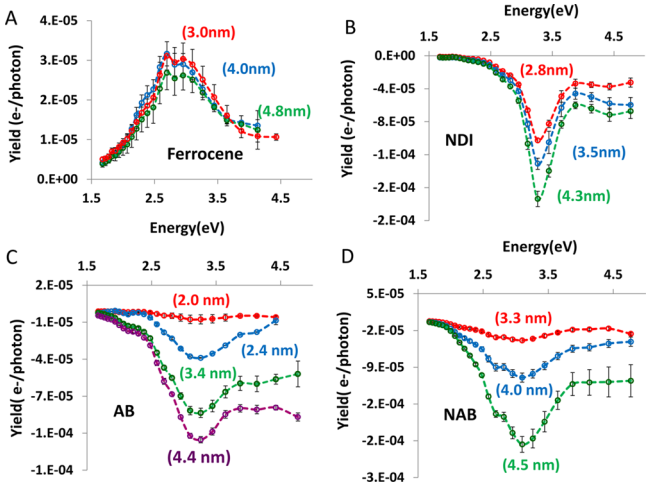

Figure 7. Photocurrent yield spectra for increasing molecular layer thicknesses, as indicated: (A) ferrocene, (B) NDI, (C) AB, (D) NAB.

the photocurrent yield spectra for junctions with molecular layer thicknesses in the 3−5 nm range for Fc NDI, AB, and NAB. For ferrocene molecules within the IPE regime (i.e., at energies less than 3 eV), the photocurrent yield is independent of molecular thickness (within experimental error), indicating that a greater path length for optical absorption has no significant effect on photocurrent. Figure 7B shows a slightly different behavior for junctions containing NDI: the yield remains almost independent of molecular thickness at low energy, whereas at energies above 3 eV, yield increases considerably with molecular layer thickness.

Figure 7 also shows photocurrent yield spectra for increasing thicknesses of AB (part C) and NAB (part D) junctions for the 2−5 nm range, showing a significant dependence of yield on molecular layer thickness. Comparison of plots of yield versus thickness for all four molecules (plots shown in Supporting Information Figure S8) reveals two distinct behaviors. For cases where the absorption by the molecular layer is small (Fc, 1.82 and 3.26 eV; NDI, AB, and NAB at 1.82 eV), the yield weakly depends on thickness. When molecular absorption is significant, there is a pronounced increase in photocurrent with increasing molecular layer thickness. Considering the results from Figure 7 and Supporting Information Figure S8 together, we conclude that two different mechanisms are responsible for generating photocurrent in molecular junctions which can be distinguished by the site of optical absorption. In IPE, hot carriers generated by light absorption in one contact cross the internal system tunneling barrier, as long as they have appropriate energy, and are then collected by the second contact. In the second mechanism, carriers are generated by absorption in the molecular layer, and may be collected or undergo bimolecular recombination. It is important to note that IPE is operative to some extent in all cases, although the yield for this process is small compared to the MA process for AB and NAB for most of the spectral range examined.

Having established how to distinguish the two different regimes, we move to an analysis of junction energy level characterizations using IPE by avoiding photon energies where molecular absorption contributes significantly. Fowler plots for all of the molecules which meet the requirement of negligible molecular absorption appear in Supporting Information Figure S9, and their intercepts are listed in Table 2. Table 2 also includes $E_f - E_{HOMO}$ offsets determined with UPS and the barrier height determined from a detailed Simmons analysis of current−voltage response of completed junctions. Table 2 shows that the value obtained for barrier heights using three different methods agrees within a reasonable margin given the experimental errors inherent in each technique. It is important to note that the experimental UPS measurements were obtained from incomplete devices without top contacts, i.e., molecular layers on carbon substrates in vacuum, whereas the Fowler intercepts were obtained from complete, working devices.

Note that the Fowler intercept for AB is approximate due to insufficient data outside the molecular absorbance regime.

Table 2. Summary of Barrier Heights Obtained Using Three Different Methods

junction	IPE/Fowler[a]	UPS[b]	Simmons fit[b]
BrP(3 nm)	1.1 ± 0.1	1.5 ± 0.15	1.5 ± 0.3
AQ(3.3 nm)	1.5 ± 0.1	1.4 ± 0.1	1.4 ± 0.2
AB(3.4 nm)	0.9[c]	1.0 ± 0.1	1.1 ± 0.2
NAB(3.3 nm)	<1.4	1.2 ± 0.15	1.3 ± 0.2
Fc(4.0 nm)	1.4 ± 0.15		
NDI(3.5 nm)	1.35 ± 0.30[d]		

[a]Fowler intercept from Supporting Information Figure S9. [b]UPS ($E_f - E_{HOMO, offset}$) and Simmons barriers from ref 24. [c]Approximate, based on two points (808 and 852 nm). [d]Photocurrent for Fowler plot was negative; all others were positive.

DOI: 10.1021/ja511592s
J. Am. Chem. Soc. XXXX, XXX, XXX−XXX

Although the Fc and NDI intercepts are similar, they clearly differ in the sign of the photocurrent, with NDI exhibiting negative photocurrent near the intercept and Fc, AQ, BrP, and AB all having positive photocurrent in the same region. Since all the cases except NAB listed in Table 2 meet the criteria for IPE, the sign of the photocurrent provides unambiguous determination of the system energies responsible for the tunneling barrier. The onset of IPE occurs at the energy closest to the system Fermi level, and represents the barrier for electron or hole tunneling. On the basis of the model of IPE in Figure 1, positive photocurrent corresponds to transport mediated by the nearest HOSO, while negative photocurrent is mediated by the nearest LUSO. Therefore, NDI is a case of electron tunneling while AQ, AB, BrP, Fc, and C12 undergo hole tunneling near the Fowler threshold. Figure 8A shows the resulting energy level diagram for the Fc junction, where a positive photocurrent was measured in the IPE wavelength regime. Along with the energy level diagram, a schematic representation of IPE is shown, where an excited hole in the Cu is filled by an electron from the carbon. Figure 8B provides a contrasting IPE mechanism and energy level diagram for the NDI-containing molecular junction, where electron transport from the Cu to carbon takes place internally. These results show that IPE may be used to obtain information from working molecular junctions about the relative alignment of occupied and unoccupied molecular orbitals relative to the system Fermi level, for either LUSO-mediated (electron) tunneling or HOSO-mediated (hole) tunneling. In this model it is implicit that photoexcitation occurs predominantly in the Cu, and that IPE is the dominant mechanism, with negligible contribution from absorption by the molecular layer or by the carbon substrate. Note that Figure 8 shows the movement of only electrons, while a different convention often shows the movement of holes. An equivalent schematic could be drawn which shows holes moving in the opposite direction to that of electrons in Figure 8, with no effect on the observed current.

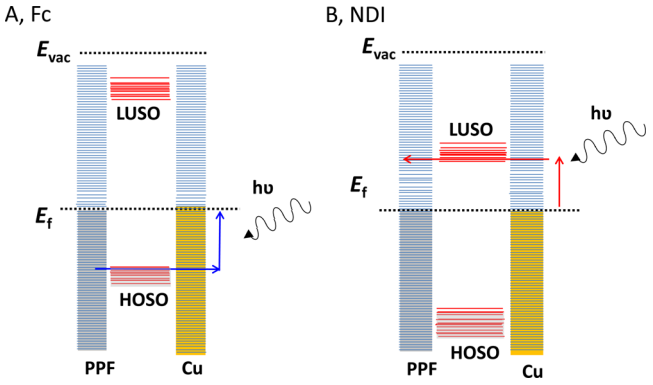

Figure 8. (A) Proposed diagram of the IPE mechanism for HOSO mediated transport of electrons from PPF to Cu for the ferrocene molecule. (B) Diagram for electron transfer from Cu to carbon through the LUSO for the NDI molecule. The alignment of the occupied system orbitals (HOSOs) and the unoccupied orbitals (LUSOs) relative to the contact Fermi levels determines the sign of the observed photocurrent and the energy threshold for onset. An equivalent figure could be drawn showing hole transport for Fc, where arrows point in the opposite direction; however, the measured current would not change.

The average tunneling barrier obtained from UPS results was 1.3 ± 0.2 eV for the aromatic molecules, quite close to the 1.2 ± 0.2 eV estimated from the $J-V$ curves using modified Simmons analysis.[45] The average tunnelling barriers obtained for the aromatic molecules by the Fowler analysis is 1.2 ± 0.2 eV, in good agreement with the previous determinations. We have previously reported the compression of interfacial barriers in our junctions,[24] due to the strong electronic coupling between the molecule and the substrate which causes a significant alteration of energy levels from those of the free molecules and unmodified substrate. Upon bonding, electronic inductive effects result in local changes in electrostatic potential and compression of the tunnelling barrier from values predicted from the free molecule energy levels. This compression has been attributed to an induced density of interface states,[65,66] sometimes referred to as the gap states,[67] which are transport states lying within the HOMO−LUMO gap of the molecular species. Such effects are a consequence of the interaction between the molecules and the contacts, and reinforce the conclusion that the entire system must be considered when predicting interfacial barriers. Therefore, direct determination of energy levels in complete, intact devices using photocurrent measurements can provide valuable information about energy level alignment, and assist in the larger problem of understanding the structural factors which determine the electronic behavior of molecular junctions.

CONCLUSIONS

This paper demonstrates that the observed photocurrent spectrum of a molecular tunnel junction is often composed of two types of photocurrent: one involving an IPE process, which can be useful for determining energy level alignment and interfacial energy barriers, and one that involves optical absorption by the molecular layer. IPE occurs when the molecular layer absorption is weak, and IPE photocurrent is linear with light intensity and weakly dependent on molecular layer thickness. The Fowler plot for IPE is linear, with its intercept on the abscissa equal to the energy offset between the system Fermi level and the nearest orbital, with positive photocurrent indicating LUSO-mediated transport and negative photocurrent indicating HOSO mediation. Chemisorbed molecules which absorb photons within the molecular layer lead to additional photocurrent, which is nonlinear with light intensity and dependent on molecular layer thickness. Although the additional photocurrent can complicate the IPE analysis, it is directly relevant to photovoltaic devices with much thicker molecular layers than those studied here. Current investigations include IPE experiments with thicker molecular layers to determine how far the photoelectron can travel before scattering within the molecular junction. In addition, the characteristics of the molecular absorption mechanism are being studied to determine its underlying mechanism. In addition to identifying the charge carrier and tunneling barriers from IPE, the alternative mechanism involving molecular absorption should reveal new photoeffects and possibly additional applications of molecular junctions in photonics.

ASSOCIATED CONTENT

Supporting Information

Experimental schematics, optical absorption spectra, photocurrent dependence on light intensity, molecular layer thickness dependence, and Fowler plots. This material is available free of charge via the Internet at http://pubs.acs.org.

DOI: 10.1021/ja511592s
J. Am. Chem. Soc. XXXX, XXX, XXX−XXX

AUTHOR INFORMATION

Corresponding Authors

adam.bergren@nrc.ca
richard.mccreery@ualberta.ca

Notes

The authors declare no competing financial interest.

ACKNOWLEDGMENTS

This work was supported by the University of Alberta, the National Research Council of Canada, the National Science and Engineering Research Council, and Alberta Innovates. We thank Bryan Szeto for expert assistance with LabView programming.

REFERENCES

(1) Tour, J. M. *Acc. Chem. Res.* **2000**, *33*, 791.
(2) Jortner, J.; Ratner, M. *Molecular Electronics*; Blackwell Science Ltd.: London, 1997.
(3) McCreery, R. L.; Bergren, A. J. *Adv. Mater.* **2009**, *21*, 4303.
(4) Akkerman, H. B.; Boer, B. d. *J. Phys.: Condens. Matter* **2008**, *20*, 013001.
(5) Cardamone, D. M.; Stafford, C. A.; Mazumdar, S. *Nano Lett.* **2006**, *6*, 2422.
(6) Chen, F.; Hihath, J.; Huang, Z.; Li, X.; Tao, N. J. *Annu. Rev. Phys. Chem.* **2007**, *58*, 535.
(7) Danilov, A.; Kubatkin, S.; Kafanov, S.; Hedegard, P.; Stuhr-Hansen, N.; Moth-Poulsen, K.; Bjornholm, T. *Nano Lett.* **2008**, *8*, 1.
(8) Huang, Z. F.; Chen, F.; Bennett, P. A.; Tao, N. J. *J. Am. Chem. Soc.* **2007**, *129*, 13225.
(9) Moth-Poulsen, K.; Bjornholm, T. *Nat. Nanotechnol.* **2009**, *4*, 551.
(10) Thieblemont, F.; Seitz, O.; Vilan, A.; Cohen, H.; Salomon, E.; Kahn, A.; Cahen, D. *Adv. Mater.* **2008**, *20*, 3931.
(11) Vilan, A.; Yaffe, O.; Biller, A.; Salomon, A.; Kahn, A.; Cahen, D. *Adv. Mater.* **2010**, *22*, 140.
(12) Luo, L.; Choi, S. H.; Frisbie, C. D. *Chem. Mater.* **2011**, *23*, 631.
(13) Aviram, A.; Ratner, M. A. *Chem. Phys. Lett.* **1974**, *29*, 277.
(14) Flood, A. H.; Stoddart, J. F.; Steuerman, D. W.; Heath, J. R. *Science* **2004**, *306*, 2055.
(15) Heath, J. R.; Ratner, M. A. *Phys. Today* **2003**, *56*, 43.
(16) Lindstrom, C. D.; Muntwiler, M.; Zhu, X. Y. *J. Phys. Chem. B* **2005**, *109*, 21492.
(17) McCreery, R. L. *Chem. Mater.* **2004**, *16*, 4477.
(18) McCreery, R. L. *Anal. Chem.* **2006**, *78*, 3490.
(19) Mirkin, C. A.; Ratner, M. A. *Annu. Rev. Phys. Chem.* **1992**, *43*, 719.
(20) Rakshit, T.; Liang, G.; Ghosh, A.; Datta, S. *Nano Lett.* **2004**, *4*, 1803.
(21) Holmlin, R. E.; Haag, R.; Chabinyc, M. L.; Ismagilov, R. F.; Cohen, A. E.; Terfort, A.; Rampi, M. A.; Whitesides, G. M. *J. Am. Chem. Soc.* **2001**, *123*, 5075.
(22) Bergren, A. J.; Harris, K. D.; Deng, F.; McCreery, R. *J. Phys.: Condens. Matter* **2008**, *20*, 374117.
(23) McCreery, R.; Yan, H.; Bergren, A. *Phys. Chem. Chem. Phys.* **2013**, *15*, 1065.
(24) Sayed, S. Y.; Fereiro, J. A.; Yan, H.; McCreery, R. L.; Bergren, A. J. *Proc. Natl. Acad. Sci. U.S.A.* **2012**, *109*, 11498.
(25) *Charge and Exciton Transport through Molecular Wires*; Siebbeles, L. D. A., Grozema, F. C., Eds.; Wiley-VCH: Weinheim, Germany, 2011.
(26) Bonifas, A. P.; McCreery, R. L. *Chem. Mater.* **2008**, *20*, 3849.
(27) Bonifas, A. P.; McCreery, R. L. *Anal. Chem.* **2012**, *84*, 2459.
(28) Scott, A.; Hacker, C. A.; Janes, D. B. *J. Phys. Chem. C* **2008**, *112*, 14021.
(29) Seitz, O.; Dai, M.; Aguirre-Tostado, F. S.; Wallace, R. M.; Chabal, Y. J. *J. Am. Chem. Soc.* **2009**, *131*, 18159.
(30) Donley, C. L.; Blackstock, J. J.; Stickle, W. F.; Stewart, D. R.; Williams, R. S. *Langmuir* **2007**, *23*, 7620.
(31) Mahmoud, A. M.; Bergren, A. J.; McCreery, R. L. *Anal. Chem.* **2009**, *81*, 6972.
(32) Nowak, A. M.; McCreery, R. L. *J. Am. Chem. Soc.* **2004**, *126*, 16621.
(33) Yoon, H. P.; Maitani, M. M.; Cabarcos, O. M.; Cai, L.; Mayer, T. S.; Allara, D. L. *Nano Lett.* **2010**, *10*, 2897.
(34) Malen, J. A.; Doak, P.; Baheti, K.; Tilley, T. D.; Majumdar, A.; Segalman, R. A. *Nano Lett.* **2009**, *9*, 3406.
(35) Malen, J. A.; Doak, P.; Baheti, K.; Tilley, T. D.; Segalman, R. A.; Majumdar, A. *Nano Lett.* **2009**, *9*, 1164.
(36) Leng, J.-C.; Lin, L. L.; Song, X.-N.; Li, Z.-L.; Wang, C.-K. *J. Phys. Chem. C* **2009**, *113*, 18353.
(37) Wang, W.; Scott, A.; Gergel-Hackett, N.; Hacker, C. A.; Janes, D. B.; Richter, C. A. *Nano Lett.* **2008**, *8*, 478.
(38) Kim, B.; Choi, S. H.; Zhu, X. Y.; Frisbie, C. D. *J. Am. Chem. Soc.* **2011**, *133*, 19864.
(39) Qi, Y.; Yaffe, O.; Tirosh, E.; Vilan, A.; Cahen, D.; Kahn, A. *Chem. Phys. Lett.* **2011**, *511*, 344.
(40) Powell, R. *J. Appl. Phys.* **1970**, *41*, 2424.
(41) Gundlach, K. H.; Kadlec, J. *J. Appl. Phys.* **1975**, *46*, 5286.
(42) DiMaria, D. J.; Arnett, P. C. *Appl. Phys. Lett.* **1975**, *26*, 711.
(43) Goodman, A. M. *J. Appl. Phys.* **1970**, *41*, 2176.
(44) Fereiro, J. A.; McCreery, R. L.; Bergren, A. J. *J. Am. Chem. Soc.* **2013**, *135*, 9584.
(45) Bergren, A. J.; McCreery, R. L.; Stoyanov, S. R.; Gusarov, S.; Kovalenko, A. *J. Phys. Chem. C* **2010**, *114*, 15806.
(46) Anariba, F.; McCreery, R. L. *J. Phys. Chem. B* **2002**, *106*, 10355.
(47) McGovern, W. R.; Anariba, F.; McCreery, R. L. *J. Electrochem. Soc.* **2005**, *152*, E176.
(48) Ranganathan, S.; McCreery, R. L.; Majji, S. M.; Madou, M. *J. Electrochem. Soc.* **2000**, *147*, 277.
(49) Yan, H.; Bergren, A. J.; McCreery, R. L. *J. Am. Chem. Soc.* **2011**, *133*, 19168.
(50) Braun, S.; Salaneck, W. R.; Fahlman, M. *Adv. Mater.* **2009**, *21*, 1450.
(51) Cahen, D.; Kahn, A. *Adv. Mater.* **2003**, *15*, 271.
(52) Ishii, H.; Sugiyama, K.; Ito, E.; Seki, K. *Adv. Mater.* **1999**, *11*, 605.
(53) Afanas'ev, V. V. *Internal Photoemission Spectroscopy: Principles and Applications*; Elsevier: Amsterdam, 2008.
(54) Goodman, A. M. *Phys. Rev.* **1966**, *152*, 780.
(55) Powell, R. J. *J. Appl. Phys.* **1969**, *40*, 5093.
(56) Mukherjee, S.; Libisch, F.; Large, N.; Neumann, O.; Brown, L. V.; Cheng, J.; Lassiter, J. B.; Carter, E. A.; Nordlander, P.; Halas, N. J. *Nano Lett.* **2013**, *13*, 240.
(57) Knight, M. W.; Sobhani, H.; Nordlander, P.; Halas, N. J. *Science* **2011**, *332*, 702.
(58) Goykhman, I.; Desiatov, B.; Khurgin, J.; Shappir, J.; Levy, U. *Nano Lett.* **2011**, *11*, 2219.
(59) Fowler, R. H. *Phys. Rev.* **1931**, *38*, 45.
(60) Sze, S. M. *Physics of Semiconductor Devices*, 2nd ed.; Wiley: New York, 1981.
(61) Tian, H.; Bergren, A. J.; McCreery, R. L. *Appl. Spectrosc.* **2007**, *61*, 1246.
(62) Cahen, D.; Kahn, A.; Umbach, E. *Mater. Today* **2005**, *8*, 32.
(63) Huynh, W. U.; Dittmer, J. J.; Teclemariam, N.; Milliron, D. J.; Alivisatos, A. P. *Phys. Rev. B* **2003**, *67*, 115326.
(64) Taylor, J. R. *An Introduction to Error Analysis*; University Science Books: Sausalito, CA, 1982; p 181.
(65) Shen, C.; Kahn, A. *Org. Electron.* **2001**, *2*, 89.
(66) Segev, L.; Salomon, A.; Natan, A.; Cahen, D.; Kronik, L. *Phys. Rev. B* **2006**, *74*, 165323.
(67) Zhong, S.; Zhong, J. Q.; Mao, H. Y.; Zhang, J. L.; Lin, J. D.; Chen, W. *Phys. Chem. Chem. Phys.* **2012**, *14*, 14127.

DOI: 10.1021/ja511592s
J. Am. Chem. Soc. XXXX, XXX, XXX−XXX